Phys Chem Minerals (1998) 26:63–77

ORIGINAL PAPER

P.R.L. Welche · V. Heine · M.T. Dove

Negative thermal expansion in beta-quartz

Received August 14 1997 / Revised, accepted January 26 1998

Abstract Computer modelling and theoretical analysis are used to explain the nearly zero and slightly negative coefficients of thermal expansion in β-quartz well above the α-β phase transition temperature. Quartz was selected for study as an archetypal material with a framework structure of stiff units, namely SiO_4 tetrahedra, linked through shared oxygen atoms as very flexible hinges. The contributions of the soft mode, the Vallade mode, the TA_z phonon branch and the phonon spectrum as a whole are discussed in detail. The results fully support and illustrate a recent theory of the negative contribution to thermal expansion in framework structures. It is a geometrical effect due to the rotation of the tetrahedral units, folding together as they vibrate. The very rapid increase in the lattice parameters for about 20 K above the transition temperature is well accounted for within quasiharmonic theory, and is therefore not evidence for critical fluctuations or fluctuating patches of α_+, α_- structure.

Introduction

Ceramics that withstand thermal shock are technologically important. Such materials need to have ultra-low coefficients of thermal expansion α (Hummel 1984), and others even have negative α at least in some crystallographic directions e.g., cordierite (Hochella and Brown 1986), β-eucryptite (Tscherry et al. 1972; Schulz 1974), dehydrated analcime (Korthuis et al. 1995; Pryde et al. 1996; Evans et al. 1997). A recent theory (Heine et al. 1998) has shown how a negative contribution arises as a geometrical effect in framework structures. By a framework structure we mean one consisting of rather stiff tetrahedral or octahedral units such as SiO_4, AlO_6, jointed into a framework by shared oxygen (or other) atoms at their corners. The geometrical negative contribution to α arises from the rotational oscillation of these units under thermal agitation. It contrasts with the normal positive expansion due to the anharmonicity of interatomic forces (Ashcroft and Mermin 1981; Downs et al. 1992). Where the observed α is very small, we can infer the existence of a negative contribution such as discussed here, on top of the normal positive anharmonic part.

The purpose of the present work is a computational study of thermal expansion in β-quartz as the first detailed case study of the negative geometrical effect, which in fact turned up a couple of surprises mentioned below.

The origin of the geometrical negative contribution to α can be seen qualitatively from Fig. 1 depicting what we shall term '2D (two dimensional) perovskite'. It is of course a section through the octahedra of the real 3D-perovskite structure, but we shall regard it more simply as a 2D structure of squares. The tetrahedral or/and octahedral units of framework structures are usually very stiff, but are rather loosely jointed at the shared corner atoms with a bond bending force constant at the corners as much as a hundred times smaller than the stiffness of the units. The coherent set of rotations depicted in Fig. 1 preserves nearly or exactly the sizes of the units, while reducing the space between them and reducing the lattice constant as the units fold together under the rotations. We have for the area of the 2D unit cell at rotation angle θ

$$A(\theta) = A_0 \cos^2\theta \approx A_0\left(1 - \eta_A \theta^2\right), \tag{1}$$

where η_A is a geometrical constant (equal to unity in this case) specific to the mode of rotation, so that at temperature T we can write

$$A(T) = A_0\left(1 - \eta_A \langle\theta^2\rangle_T\right). \tag{2}$$

As the temperature increases, the amplitude of thermal agitation increases. Thus the thermal average $\langle\theta^2\rangle_T$ increases with T, and the unit cell area (Eq. 1) decreases, giving a negative coefficient of thermal expansion. We can carry this very qualitative picture a little further.

P.R.L. Welche · V. Heine
Theory of Condensed Matter, Cavendish Laboratory, Madingley Road, Cambridge CB3 0HE, UK

M.T. Dove (✉)
Dept. of Earth Sciences, University of Cambridge, Downing Street, Cambridge CB2 3EQ, UK

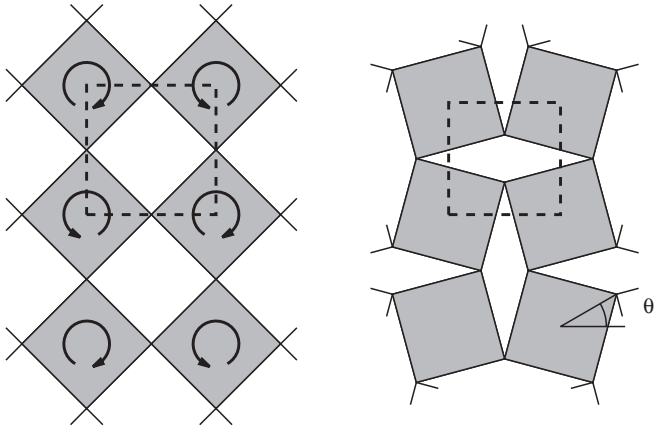

Fig. 1 Rotational motion in '2D-perovskite', showing the rotation of the units by an angle θ. Note the reduction, due to the rotation, of the size of the square unit cell (*dashed*)

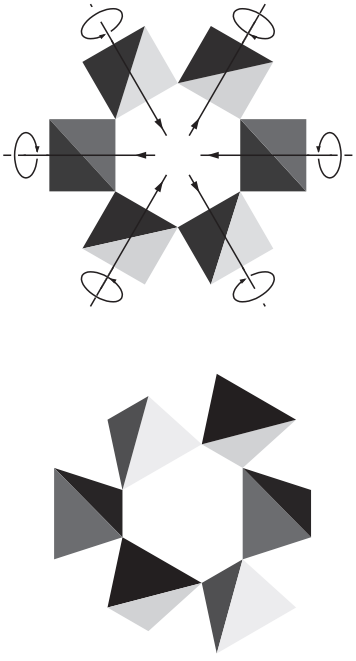

Fig. 2 The structure of β-quartz (top) projected onto the *ab* plane, and of α-quartz (bottom) derived from β-quartz by freezing in the soft mode consisting of rotations of the tetrahedra by an angle θ about the axes shown

The value $\langle\theta^2\rangle_T$ can be derived easily from the theory of simple harmonic motion and the principle of equipartition of energy. Quite generally in simple harmonic motion, the frequency squared, ω^2, is the ratio of the restoring force constant to the inertia coefficient. Thus for rotational oscillations at temperature T we have potential energy

$$V = \tfrac{1}{2} I \omega^2 \langle\theta^2\rangle_T = \tfrac{1}{2} k_B T \tag{3}$$

where I is the moment of inertia of the square, tetrahedron or octahedron and k_B is Boltzmann's constant. Thus we have for the area in Fig. 1

$$A(T) = A_0 \left(1 - \eta_A \frac{k_B T}{I \omega^2}\right). \tag{4}$$

The thermal expansion coefficient

$$\alpha = -\eta_A \frac{k_B}{I \omega^2} \tag{5}$$

is thus negative. We shall term this our geometrical effect because it arises from simple rotations of the units with the value of η determined by geometrical considerations. Equation (5) already makes the important point that a low ω leads to a large effect.

Figure 1 and Eq. 5 indicate the connection between negative expansion and recent work on what are called 'floppy modes' (Dove et al. 1997) and Rigid Unit Modes (RUMs) (Dove et al. 1991, 1992, 1995; Hammonds et al. 1996). The rotation in Fig. 1 can be achieved without any distortion of the stiff units and is therefore an example of a RUM. With the bond bending force constants between the units at the corners being so weak, we expect such RUMs to have a very low frequency and hence from (Eq. 5) to give a strong negative contribution to α. RUMs are involved in other physical processes, particularly as pathways for many displacive phase transitions, e.g., in perovskites the mode depicted in Fig. 1 (Hammonds et al. 1996). They can also determine cation ordering in silicates, give diffuse X-ray and electron scattering (Dove et al. 1996) and hold catalyst ions in zeolites (Hammonds et al. 1997a, b, 1998).

In the present work, β-quartz has been chosen for a quantitative study of a material with negative α, in order to document in detail our ideas about the geometrical origin of the negative effect. It is about the simplest tetrahedral framework material, and its lattice vibrations have been well studied in relation to RUMs (Dove et al. 1991, 1995). Indeed it was the study of the incommensurate phase of quartz (occuring over a range of 1.5 K between the α and β phases) which first prompted the general study of RUMs (Tautz et al. 1991; Vallade et al. 1992). The coherent rotation of tetrahedra leading from β-quartz to the α form (Fig. 2) is a RUM, which we shall refer to as the soft mode (SM), so that quartz would enable one to see the special role of the soft mode involved in a phase change. Moreover there is a well tested expression for the interatomic forces in SiO_2 (Tsuneyuki et al. 1988) as a basis for studying the lattice vibrations computationally. The experimental data for the expansion of β-quartz are shown in Fig. 3, where it is convenient not to plot α but the actual changes of the a and c lattice parameters as measured by precision neutron diffraction (Carpenter et al. 1998). We note indications above 860 K of a small contraction in c and practically zero expansion in a. As mentioned before, we take zero expansion as an indication of the negative geometrical contribution on top of the normal anharmonic positive expansion. The soft mode in the β-phase leads to a contraction exactly analogous to that in Fig. 1. This is bound to be so because the high symmetry β-structure has to have maxi-

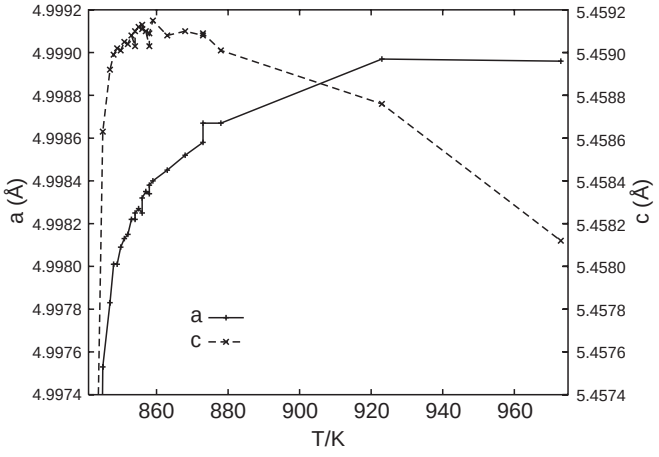

Fig. 3 Experimental data on lattice parameters after Carpenter et al. (1998). The α-β transition temperature is, as closely as can be defined, at the left hand edge of the figure at 841 K

mum volume by symmetry, with a decrease in volume as the tetrahedra fold up together from the rotations. Thus the α-structure has lower volume than β-quartz, and both a and c lattice parameters increase with increasing T in the α-phase as the order parameter (angle of rotation from the hexagonal β-quartz) decreases. This change is enormous on the scale of Fig. 3, where we are concerned only with the effect of rotational fluctuations in the hexagonal β-structure. To see our geometrical fluctuation effect in the lattice expansion we therefore had to go to β-quartz, and not the α-phase where our effect is swamped by the static structural change.

The present paper presents a detailed calculation of the thermal expansion of β-quartz and its interpretation in terms of the geometrical picture and theory introduced in simplified form in Fig. 1 and Eqs. 4 and 5. The traditional theory of lattice expansion which we shall call the Grüneisen theory is presented briefly in the next Section, expressed in terms of the reduced Grüneisen constant

$$\gamma_{\mathrm{c}}^{\mathrm{red}}(\mathbf{k}j) = -\frac{1}{2}\frac{\partial\omega_{\mathbf{k}j}^2}{\partial e_{\mathrm{c}}} \tag{6a}$$

for the phonon mode of wave vector $\mathbf{k}$ in phonon band j where e_{c} is the strain $\delta c/c$, and similarly

$$\gamma_{\mathrm{ab}}^{\mathrm{red}}(\mathbf{k}j) = -\frac{1}{2}\frac{\partial\omega_{\mathbf{k}j}^2}{\partial e_{\mathrm{ab}}} \tag{6b}$$

where e_{ab}=$\delta a/a$ for varying the a and b lattice parameters simultaneously keeping the hexagonal symmetry. These reduced Grüneisen constants γ^{red} are simply related to the more conventional Grüneisen constants γ by

$$\gamma_{\mathrm{c}}(\mathbf{k}j) = \omega_{\mathbf{k}j}^{-2}\gamma_{\mathrm{c}}^{\mathrm{red}}(\mathbf{k}j), \tag{7a}$$

$$\gamma_{\mathrm{ab}}(\mathbf{k}j) = \omega_{\mathbf{k}j}^{-2}\gamma_{\mathrm{ab}}^{\mathrm{red}}(\mathbf{k}j). \tag{7b}$$

The phonon bands $\omega_{\mathbf{k}j}^2$ are computed from the interatomic forces and hence the $\gamma^{\mathrm{red}}(\mathbf{k}\,j)$ by varying the lattice parameters as we will see in the section on computational methods and results. The contribution of each phonon mode to the thermal expansion is expressed in terms of its $\gamma^{\mathrm{red}}(\mathbf{k}\,j)$ and the result summed. This formulation includes everything, i.e., both the negative geometrical contribution and the positive anharmonic part. But the geometrical effect (alone) can also be expressed in terms of calculable geometrical constants $\eta_{\mathrm{ab}}(\mathbf{k}\,j)$, $\eta_{\mathrm{c}}(\mathbf{k}\,j)$ analogous to η_{A} in Eq. 1 (Heine et al. 1998), and we shall interpret some of the $\gamma^{\mathrm{red}}(\mathbf{k}\,j)$ in terms of them in the Section on discussion of the computed Grüneisen constants, particularly for the soft mode and for the $\mathrm{TA_z}$ modes for $\mathbf{k}$ in the a^* direction, as well as the general pattern of $\gamma^{\mathrm{red}}(\mathbf{k}\,j)$ through the bands. One of the surprises was that the largest negative contribution comes from the $\mathrm{TA_z}$ modes, which are also RUMs. We should emphasise that RUMs are just a few special modes along special lines and planes in the Brillouin zone. If we think in terms of translations and rotations of tetrahedra, we can say that half the phonon spectrum is concerned with rotations and indeed the $\eta(\mathbf{k}\,j)$ are comparable throughout the whole spectrum. It is the ω^{-2} weighting factor in Eq. 4 that gives a particular emphasis to the RUMs and nearly-RUMs. The total results for the thermal expansion will be presented and interpreted semiquantitatively in later sections.

At the outset of the present work it was thought that the soft mode would make the dominant negative contribution to the expansion. It is a RUM, gives contractions in both a and c analogous to Eq. 1, and has a low frequency in the β-phase which in fact goes to zero as T approaches T_{c} (Tezuka et al. 1991):

$$\frac{\omega_{\mathrm{SM}}^2(T)}{4\pi^2} = 2.122\times10^{-3}(T-T_{\mathrm{c}})\,(\mathrm{THz})^2, \quad T\,\mathrm{in\,K}. \tag{8}$$

At the same time it was thought that the rapid rise in a and c in Fig. 3 in the range of 20 degrees above T_{c} was some precursor of the phase transition associated with critical fluctuations or otherwise beyond the scope of the present theory. This view turns out to be mistaken. The full theory also takes into account the temperature dependence of ω^2 as in Eq. 8, which turns a negative effect into a positive one and accounts for the rapid expansion above T_{c}: see the Section on the contribution of the soft mode band, and our overall conclusions in final section.

Theory

In this section, we derive equations for thermal expansion and strain suitable for use within a lattice dynamics computation, i.e., in terms of phonon frequencies in the quasiharmonic approximation. The derivations are restricted to the particular case of β-quartz which is hexagonal (space group $\mathrm{P_6222}$).

We start by considering the free energy of the crystal in the quasi-harmonic approximation (Leibfried and Ludwig 1961)

$$G = G_{\rm el} + G_{\rm vib} \tag{9}$$

as a sum of an elastic term $G_{\rm el}$ and the vibrational free energy $G_{\rm vib}$. Both of these are written for arbitrary strains $e_{\rm ab}$, $e_{\rm c}$ so that by minimising Eq. 9, one can determine the temperature variations of $e_{\rm ab}(T)$ and $e_{\rm c}(T)$ and hence the thermal expansion. To maintain hexagonal symmetry, the a and b lattice parameters are always varied together in our calculations, and $e_{\rm ab}$ is defined as

$$e_{\rm a} = \frac{\delta a}{a} = e_{\rm b} = \frac{\delta b}{b} = e_{\rm ab}. \tag{10}$$

In the quasi-harmonic approximation, $G_{\rm vib}$ is the free energy of an ensemble of simple harmonic oscillators, but with temperature and strain dependent frequencies (Dove 1993),

$$G_{\rm vib}(e_{\rm ab}, e_{\rm c}, T) = \frac{k_{\rm B}T}{N\upsilon}\sum_{\mathbf{k}j} \ln\left[2\sinh\left(\frac{\hbar\,\omega_{\mathbf{k}j}(e_{\rm ab}, e_{\rm c}, T)}{2k_{\rm B}T}\right)\right]. \tag{11}$$

Here we have considered a sample which has unit equilibrium volume at zero Kelvin and contains N cells of volume υ each. Also we use periodic boundary conditions, and $\omega_{\mathbf{k}j}$ is the frequency of the $j^{\rm th}$ mode at wave vector $\mathbf{k}$ in the Brillouin zone. It has been proved that this procedure gives a good account of the thermal expansion taking anharmonicity into account (Leibfried and Ludwig 1961).

The elastic energy for the hexagonal crystal is

$$G_{\rm el}(e_{\rm ab}, e_{\rm c}) = (c_{11}+c_{12})\,e_{\rm ab}^2 + 2c_{13}e_{\rm ab}\,e_{\rm c} + \tfrac{1}{2}c_{33}e_{\rm c}^2 + \text{terms involving shear.} \tag{12}$$

Minimising the total free energy with respect to $e_{\rm ab}$ strain, we find

$$\left.\frac{\partial G}{\partial e_{\rm ab}}\right|_{e_{\rm c},T} = 0 = 2(c_{11}+c_{12})\,e_{\rm ab} + 2c_{13}e_{\rm c} - \frac{1}{N\upsilon}\sum_{\mathbf{k}j} E_{\mathbf{k}j}\frac{1}{\omega_{\mathbf{k}j}^2}\gamma_{\rm ab}^{\rm red}(\mathbf{k}j) \tag{13}$$

where

$$E_{\mathbf{k}j} = \left(n_{\mathbf{k}j} + \tfrac{1}{2}\right)\hbar\,\omega_{\mathbf{k}j} \tag{14}$$

is the energy of the $\mathbf{k}\,j^{\rm th}$ oscillator (equal to $k_{\rm B}T$ in the high temperature limit), where

$$n_{\mathbf{k}j} = \left(e^{\beta\hbar\omega_{\mathbf{k}j}} - 1\right)^{-1} \tag{15}$$

is the usual Bose-Einstein distribution (β=1/$k_{\rm B}T$). The reduced Grüneisen constant $\gamma_{\rm ab}^{\rm red}$ and its relation to the more usual Grüneisen constant $\gamma_{\rm ab}$ have been defined in Eqs. 6 and 7. Similarly minimising the free energy with respect to $e_{\rm c}$, keeping a and b fixed, yields

$$\left.\frac{\partial G}{\partial e_{\rm c}}\right|_{e_{\rm ab},T} = 0 = 2c_{13}e_{\rm ab} + c_{33}e_{\rm c} - \frac{1}{N\upsilon}\sum_{\mathbf{k}j} E_{\mathbf{k}j}\frac{1}{\omega_{\mathbf{k}j}^2}\gamma_{\rm c}^{\rm red}(\mathbf{k}j). \tag{16}$$

Solving the simultaneous equations 13 and 16, we obtain

$$e_{\rm ab}(T) = \frac{c_{33}\left(\frac{1}{2}\xi_{\rm ab}\right) - c_{13}e_{\rm c}}{(c_{11}+c_{12})\,c_{33} - 2c_{13}^2} \tag{17a}$$

and

$$e_{\rm c}(T) = \frac{(c_{11}+c_{12})\,\xi_{\rm c} - 2c_{13}\left(\frac{1}{2}\xi_{\rm ab}\right)}{(c_{11}+c_{12})\,c_{33} - 2c_{13}^2} \tag{17b}$$

where

$$\xi_{\rm ab}(T) = \frac{1}{N\upsilon}\sum_{\mathbf{k}j} E_{\mathbf{k}j}\frac{1}{\omega_{\mathbf{k}j}^2}\gamma_{\rm ab}^{\rm red}(\mathbf{k}j) \tag{18a}$$

and

$$\xi_{\rm c}(T) = \frac{1}{N\upsilon}\sum_{\mathbf{k}j} E_{\mathbf{k}j}\frac{1}{\omega_{\mathbf{k}j}^2}\gamma_{\rm c}^{\rm red}(\mathbf{k}j) \tag{18b}$$

are thermal stresses.

Equation 17 gives the thermal expansion in the $a\,b$ plane and in the c direction, from which the coefficients of expansion $\alpha_{\rm a}$=$\alpha_{\rm b}$=$\alpha_{\rm ab}$ and $\alpha_{\rm c}$ are obtained by differentiating with respect to T:

$$\alpha_{\rm a} = \frac{{\rm d}e_{\rm ab}(T)}{{\rm d}T}, \tag{19a}$$

$$\alpha_{\rm c} = \frac{{\rm d}e_{\rm c}(T)}{{\rm d}T}. \tag{19b}$$

We can check that the theory reduces to the usual formula (Ashcroft and Mermin 1981)

$$\alpha = \frac{c_{\rm V}\gamma}{3B} \tag{20}$$

for the coefficient of expansion α of an isotropic material where B is the bulk modulus and $c_{\rm V}$ the specific heat per unit volume. The conventional Grüneisen parameter

$$\gamma = -\left.\frac{\partial \ln\omega}{\partial \ln V}\right|_{P,T} = \frac{1}{\omega^2}\cdot -\frac{1}{2}\left.\frac{\partial\omega^2}{\partial e_{\rm V}}\right|_{P,T} = \frac{1}{\omega^2}\gamma^{\rm red} \tag{21}$$

is assumed to apply to all phonon modes equally. For an isotropic material c_{11}=c_{33} and c_{12}=c_{13}, and B is given by

$$B = \tfrac{1}{3}(c_{11}+2c_{12}). \tag{22}$$

We also have

$$\gamma = \gamma_{\rm c} = \tfrac{1}{2}\gamma_{\rm ab} \tag{23}$$

whence Eq. 17 reduces to

$$e_{\rm ab}(T) = e_{\rm c}(T) = e(T) = E_V(T)\,\gamma/3B \tag{24}$$

where

$$E_V(T) = \frac{1}{Nv}\sum_{\mathbf{k}j} E_{\mathbf{k}j}(T) \tag{25}$$

is the total thermal energy of the phonons per unit volume. The result (Eq. 20) now follows on differentiating Eq. 24 with respect to T.

Computational method and results for the Grüneisen constants

To calculate the thermal expansion from Eqs. 17 and 18, we need to compute the phonon frequencies $_{\mathbf{k}j}$ and the reduced Grüneisen constants $\gamma_{ab}^{red}(\mathbf{k}j)$, $\gamma_c^{red}(\mathbf{k}j)$. The latter from Eq. 6 must be obtained by calculating $\omega_{\mathbf{k}j}^2$ at two different lattice parameters (a_0, c_0) and ($a_0+\delta a$, c_0) for γ_{ab}^{red} or (a_0, $c_0+\delta c$) for γ_c^{red}. The chosen strain was of the order of 0.01%.

These frequencies were computed by a lattice dynamics simulation, taking the β-quartz structure shown in Fig. 2 of space group $P6_222$ and relaxing it at each (a, c) using a slightly modified version of the programme wmin (Busing 1981). The phonon spectrum of the relaxed structure was computed with the programme thbphon (Pavlides and Catlow 1993) using the Tsuneyuki et al. (1988) pair potentials. These are known to give a good representation of the interatomic forces for SiO_2, and the phonon spectra obtained match those of Dolino et al. (1992) and account for the incommensurate structure (Tautz et al. 1991).

To obtain γ_{ab}^{red}, γ_c^{red}, the strained and equilibrium phonon spectra were differenced. Some results for $\mathbf{k}$=0 are given in Table 1. When a or c changes, $\mathbf{k}$ changes, so some care must be taken about which $\omega_{\mathbf{k}j}(a_0, c_0)$ to associate with which $\omega_{\mathbf{k}(a,c)j}(a, c)$. It is clear from Eqs. 10, 13 and 16 that we want the change of a given mode with a or c. With periodic (Born-von Kàrmàn) boundary conditions on a sample of $N_a \times N_b \times N_c$ unit cells, the $\mathbf{k}$-vectors of the modes are

$$\mathbf{k}=k_a\mathbf{a}^*+k_b\mathbf{b}^*+k_c\mathbf{c}^* \tag{26}$$

where

$$k_a=n_a/N_a, \qquad 0\le n_a<N_a \text{ etc.} \tag{27}$$

Hence when a or c changes, we difference modes of the same k_a etc.

As an intermediate result, the phonon spectrum at $\mathbf{k}$=0 is shown in Fig. 4, where a and c were expanded consistently over a wide range by applying a negative pressure and relaxing. The slopes of the graph correspond directly to $-2\gamma_V^{red}(0j)$ where

$$\gamma_V^{red} = \omega^2 \cdot -\left.\frac{\partial \ln \omega}{\partial \ln V}\right|_{P,T} \approx \frac{1}{3}\left(\gamma_{ab}^{red} + \gamma_c^{red}\right). \tag{28}$$

Immediately we see that the low frequency modes have positive slopes, and therefore negative $\gamma_V^{red}(0j)$. Note that many (9 out of 27) modes have negative $\gamma_V^{red}(0j)$ (cf. Table 1), and that γ_V^{red} is independent of volume for each mode.

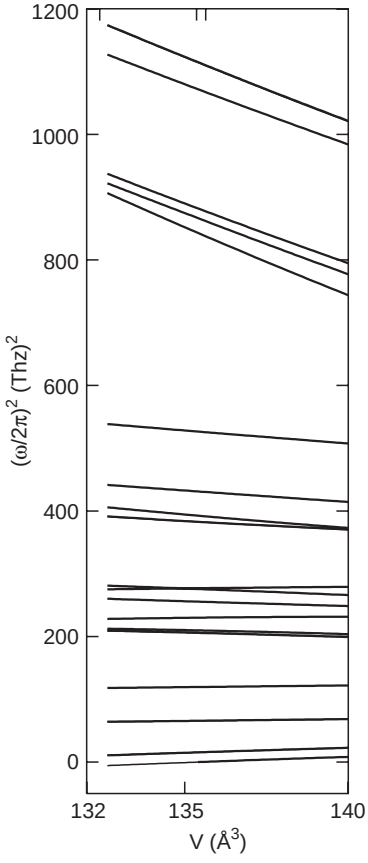

Fig. 4 Squared frequencies $\omega^2(\mathbf{k}, j)/4\pi^2$ at $\mathbf{k}$=0 at expanded cell volumes. Three particular volumes defined in the text are marked on the upper axis. Note that there are less than 27 distinct frequencies because several modes are doubly degenerate and because the three acoustic modes disappear at $\mathbf{k}$=0

The problem with lattice dynamics, especially in a thermal expansion calculation, is that the phonons can only be computed at zero Kelvin. At this temperature, β-quartz is not stable, as can be seen by the negative ω_{SM}^2 at the equilibrium volume 132.40 Å^3 in Fig. 4, and must be expanded artificially to bring it into a region of stability. Not only must ω_{SM} be real, but as phonon bands interact, eg., the SM band with TA_y along $\mathbf{a}^*$ as shown in the computed dispersion curve in Fig. 5, the structure had to be expanded to give a comparable degree of mode mixing to that known experimentally, i.e., to put $\omega_{SM}^2(T)$ where it really is. At V=135.36 Å^3 in our simulation, we have ω_{SM}=0 which corresponds to T_c. From (1.8) at 1091 K we have $\omega_{SM}{}^2/4\pi^2 = 0.53\,\text{THz}^2 4\pi^2 = 0.53\,\text{THz}^2$ as marked on Fig. 4 at V=135.64 Å^3. Clearly from Fig. 4 the variation of ω^2 is linear over this range with no mixing at $\mathbf{k}$=0 to complicate the picture, so it matters not at which particular value of (a_0, c_0) the difference is carried out. Hence we are justified in calculating Grüneisen parameters by this device of expanding the structure to give a stable phonon spectrum at zero Kelvin. To get the frequen-

Table 1 Values of $\gamma_V^{red}(\mathbf{k}j)$ at $\mathbf{k}$=0, and comparison with Eq. 32

j	$\omega/2\pi$ THz	$\frac{1}{2}\gamma_{ab}^{red}/4\pi^2$ (THz)^2 computed	$\gamma_c^{red}/4\pi^2$ (THz)^2 computed	$\gamma_V^{red}/4\pi^2$ (THz)^2 computed	$\gamma_V^{red}/4\pi^2$ (THz)^2 Eq. 32
4	0.73	−126.78	−139.48	−130.01	−180.24
5	3.99	−107.35	−129.22	−112.95	−156.61
6	3.99	−107.35	−129.22	−112.95	−156.61
7	8.12	−37.33	−42.91	−38.78	−80.07
8	8.12	−37.33	−42.91	−38.78	−80.07
9	10.94	−46.24	−8.26	−36.46	2.30
10	14.34	118.05	8.82	89.97	133.72
11	14.34	118.05	8.82	89.97	133.72
12	14.48	28.23	215.62	76.58	139.80
13	15.17	−66.05	46.82	−36.91	171.48
14	15.17	−66.05	46.82	−36.91	171.48
15	15.98	23.96	353.39	108.81	209.71
16	16.65	34.09	−248.56	−38.68	243.20
17	19.55	279.09	−52.95	193.50	404.03
18	19.55	279.09	−52.95	193.50	404.03
19	19.78	264.03	446.57	310.94	418.19
20	19.78	264.03	446.57	310.94	418.19
21	20.74	182.26	455.79	252.68	477.49
22	28.94	1447.33	1709.04	1514.48	1101.38
23	29.47	1472.15	1108.01	1378.18	1148.97
24	29.50	1209.76	1513.65	1287.90	1151.21
25	29.50	1209.76	1513.65	1287.90	1151.21
26	33.30	1442.51	1359.32	1420.90	1516.63
27	33.30	1442.51	1359.32	1420.90	1516.63

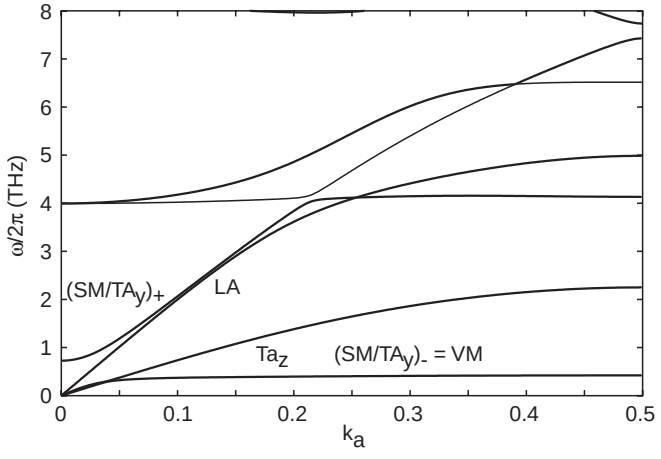

Fig. 5 Phonon frequencies for the lowest bands along the $\mathbf{k}=k_a a^*$ direction. SM=Soft Mode at $\mathbf{k}$=0, which mixes with the transverse acoustic TA_y mode polarised in the y direction for $k_a \neq 0$ to form the Vallade Mode (VM) beyond the anti-crossing. TA_z is the other transverse acoustic and LA the longitudinal acoustic branch. The volume was extended so that the calculated soft mode frequency corresponds to the actual soft mode at 1091 K

cies nearly right as a function of temperature, we adjust the volume (by applying negative pressure) to generate the correct experimental ω_{SM} as already stated: the other frequencies will then be very nearly, but not quite, right.

Another problem is that $\gamma^{red}(\mathbf{k}\,j)$, plotted in Fig. 6 along a^*, shows a hiccough when two bands cross, or 'anti-cross' (interact and hence do not cross but interchange smoothly), eg., at k_a=0.25 in Fig. 6. This is caused by $\omega^2(\mathbf{k}, j)$ being differenced with $\omega^2(\mathbf{k}, j+1)$; but the 'errors' or anomalies in the two bands cancel out in Eq. 18 because $\omega^2(\mathbf{k}, j)+\omega^2(\mathbf{k}, j+1)$ is a smooth function of a, c.

In Fig. 4 the high modes have large positive γ^{red}, but the low modes have large ω^{-2} factors to combine with their modest negative γ^{red}, so the sign of the thermal expansion coefficient of β-quartz becomes a question of balance: do the low frequency modes outweigh those with high frequency? To answer this, the full computation with summation over $\mathbf{k}$-space as per Eq. 18 is necessary. Computationally, the summation

$$\frac{1}{N}\sum_{\mathbf{k}} \quad \text{becomes} \quad \frac{1}{N_s}\sum_{\mathbf{k}_s} \tag{29}$$

where N_s is the number of sampling points $\mathbf{k}_s$ in the unit cell of reciprocal space.

Near $\mathbf{k}$=0, the acoustic modes have $\gamma^{red} \propto k^2$ and hence γ remains finite. However phonon bands vary rapidly near $\mathbf{k}$=0, and incidentally as one moves away from the a^* axis, so that one needs a large number of sampling points. The sample of points used was

$$\mathbf{k} = \frac{(2n_a-1)-N_a}{2N_a}\mathbf{a}^* + \frac{(2n_b-1)-N_b}{2N_b}\mathbf{b}^* + \frac{(2n_c-1)}{2N_c}\mathbf{c}^*, \tag{30}$$

where $1 \le n_a \le N_a$ etc., and $N_a=N_b=2N_c=N_s$. The summation was just carried out for positive c^* as it is equal to the summation over negative c^* by time reversal symmetry. Convergence tests for N_s=16–70 showed that Ns=40 was sufficient. Table 2 shows the mode Grüneisen parameter averaged over k-space according to

$$\gamma(j) = \sum_{\mathbf{k}} c_V(\mathbf{k}j)\,\gamma(\mathbf{k}j) \Big/ \sum_{\mathbf{k}} c_V(\mathbf{k}j) \tag{31}$$

for N_s=70, where c_V is the specific heat capacity of a mode.

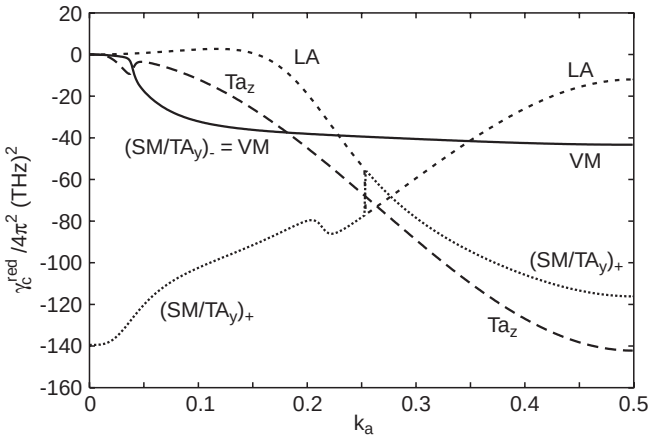

Fig. 6 Reduced Grüneisen constant $\gamma_c^{red}(\mathbf{k}, j)$ at $\mathbf{k}=k_a a^*$ for the first four bands j=1 to 4 under the same conditions as in Fig. 5

Discussion of the computed Grüneisen constants

The purpose in the present section is to give an interpretation of some of the salient results of the calculated $\gamma^{red}(\mathbf{k}\,j)$, particularly in the light of the geometrical effect outlined semiquantitatively in Eqs. 1–5, and developed systematically by Heine et al. (1998), which we refer to as Paper I.

Variation of $\gamma^{red}(\mathbf{k}\,j)$ through the phonon spectrum

In Tables 1 and 2 we see that γ^{red} and γ vary from substantial negative values for the lowest bands, to positive values at the top of the phonon spectrum. Table 1 gives γ_V^{red}at $\mathbf{k}$=0 corresponding to the gradients in Fig. 4. Table 2 shows γ averaged over each band.

In Paper I we showed that very roughly

$$\gamma^{red} \approx -A + B\omega^2, \quad A, B > 0 \tag{32}$$

through the phonon spectrum where A and B represent the geometrical and anharmonic effects respectively. This fits the results in Table 1 reasonably well with $A/4\,\pi^2$=180 THz^2, B=1.5, and gives a negative γ^{red} for low modes, going positive for higher ones.

The averaged $\gamma_{ab}(j)$ and $\gamma_c(j)$ of Table 2 are negative for the lowest 11 out of 27 bands. This large number of modes with negative γ was originally surprising because our qualitative picture before the theory of Paper I had thought in terms of RUMs and near RUMs à la Fig. 1 and Eq. 4 which are far fewer in number. The behaviour in Eq. 32, which is delved into in detail in Paper I, may be interpreted as follows. The first term, $-A$, the geometrical effect, is a reduction in area (Fig. 1) or lattice parameters which is more-or-less a local effect. This means it is a constant in k-space. It is better to think of the second term in terms of γ, where quite simply B=γ. It is a feature of the anharmonic interatomic interaction that its contribution to γ is positive and approximately independent of frequency.

Table 2 Computed Grüneisen constants for quartz averaged over the Brillouin zone for each band j according to Eq. 31

j	$\frac{1}{2}\gamma_{ab}$	γ_c	γ_V
1	−27.19	−29.52	−27.74
2	−10.19	−11.09	−10.41
3	−6.11	−6.76	−6.27
4	−3.29	−3.58	−3.37
5	−1.64	−1.75	−1.67
6	−0.92	−0.91	−0.92
7	−0.36	−0.61	−0.43
8	−0.15	−0.63	−0.27
9	−0.23	−0.63	−0.34
10	−0.24	−0.60	−0.33
11	−0.02	−0.13	−0.05
12	0.26	0.33	0.28
13	0.31	0.52	0.36
14	0.33	0.66	0.41
15	0.28	0.31	0.29
16	0.35	0.36	0.36
17	0.51	0.65	0.55
18	0.71	0.83	0.74
19	0.67	0.71	0.68
20	0.44	0.36	0.42
21	0.50	0.58	0.52
22	1.66	1.83	1.71
23	1.59	1.60	1.59
24	1.47	1.55	1.49
25	1.37	1.43	1.39
26	1.28	1.36	1.30
27	1.24	1.31	1.26

Geometrical interpretation of γ^{red} for the soft mode

The purpose of the present subsection is to show that the computed γ_{SM}^{red} for the soft mode at $\mathbf{k}$=0 can be interpreted in the geometrical way outlined in the first section. The soft mode's geometry is well understood (Megaw 1973, Grimm and Dorner 1975), so the geometrical constants, η, encountered in the introduction may be calculated explicitly. We find for the soft mode

$$\eta_{ab} = \sqrt{3}\Big/\left[2\left(1+\sqrt{3}\right)\right] = 0.317 \quad \text{and} \quad \eta_c = 1/2. \tag{33}$$

To use these η coefficients to interpret the γ_{SM}^{red} in Table 1, we need to develop the theory of Eqs. 4 and 5, to cast it in the form set out in the theory section. To be precise, the η coefficients may be related to γ^{red} by comparing Eqs. 17 and 18, with the temperature dependent part of Eq. 4 or rather the equivalent expressions for the lattice constants $a(T)$, $c(T)$. Remember that the high temperature approximation E=$k_B T$ was used in Eq. 4, so that the contributions of one mode to the strains in Eqs. 17 and 18, are of the form

$$e(\mathbf{k}j) \propto k_B T\, \omega_{\mathbf{k}j}^{-2} \gamma^{red}(\mathbf{k}j) \tag{34}$$

which is analogous to the η form of Eq. 4, namely

$$e(\mathbf{k}j) \propto k_B T\, \omega_{\mathbf{k}j}^{-2} \eta(\mathbf{k}j). \tag{35}$$

Then equating Eqs. 34 and 35 allows us to interpret a computed negative γ^{red} in Eqs. 34 in terms of an η coefficient in Eq. 35. The exact form of the relationship is derived in Paper I:

$$\gamma_s^{\mathrm{red}}(\mathbf{k}j) \approx -(\upsilon/3I)\, c_{st}\eta_t(\mathbf{k}j) \tag{36}$$

where υ is the unit cell volume, I the moment of inertia of a tetrahedron about the axis pictured in Fig. 2 which enters in Eq. 4, and the c_{st} are the elastic constants. The approximation stems from the lack of a translational component in, and therefore an underestimation of, the inertia factor, I.

The right hand side of Eq. 36 gives

$$\frac{\frac{1}{2}\gamma_{\mathrm{ab}}^{\mathrm{red}}}{4\pi^2} = -\left(\frac{\upsilon}{3I}\right)\frac{(c_{11}+c_{12})\eta_{\mathrm{ab}} + c_{13}\eta_{\mathrm{c}}}{4\pi^2}, \tag{37a}$$

$$\frac{\gamma_{\mathrm{c}}^{\mathrm{red}}}{4\pi^2} = -\left(\frac{\upsilon}{3I}\right)\frac{2c_{13}\eta_{\mathrm{ab}} + c_{33}\eta_{\mathrm{c}}}{4\pi^2}. \tag{37b}$$

We can now make a detailed comparison with the lattice dynamics results of Table 1. The pair potentials (Tsuneyuki et al. 1988) gave the following elastic constants for the expanded β-quartz used for the calculations: c_{11}=187.4 GPa, c_{12}=90.0 GPa, c_{13}=116.4 GPa, c_{33}=182.7 GPa and c_{44}=24.1 GPa. Substituting them along with V=135.65 Å^3 and I=9.7×10^{-46} kg m^2 into Eq. 37 gives

$$\tfrac{1}{2}\gamma_{\mathrm{ab}}^{\mathrm{red}}/4\pi^2 = -172(\mathrm{THz})^2$$

$$\gamma_{\mathrm{c}}^{\mathrm{red}}/4\pi^2 = -195(\mathrm{THz})^2. \tag{38}$$

These geometrical values compare reasonably with the values −127, −139 (THz)^2 in Table 1 from the lattice dynamics computation, bearing in mind that the latter include a positive contribution from the anharmonicity inherent in the pair potentials, and the approximation inherent in Eq. 36.

In conclusion, there is reasonable agreement between the values of γ^{red} computed for the soft mode in β-quartz and those calculated from the analytic geometrical constants η, which validates the whole notion of a negative geometrical effect and our Eq. 36.

Comparison with experiment for the soft mode

The α-β phase transition temperature, T_{c}, is defined by $\omega_{\mathrm{SM}}^2 = 0$, and varies with pressure and therefore with volume. This pressure variation $\partial T_{\mathrm{c}}/\partial P$ is known experimentally (Kravchuk and Tödheide 1996), so that we can deduce an experimental value for $\gamma_{\mathrm{V}}^{\mathrm{red}}$. Along the phase transition in the T–V plane, we have

$$\omega_{\mathrm{SM}}^2(T_{\mathrm{c}}, V) = 0 \tag{39}$$

$$\mathrm{d}\omega_{\mathrm{SM}}^2(T_{\mathrm{c}}, V) = 0 = \left(\frac{\partial\omega_{\mathrm{SM}}^2}{\partial T}\right)\mathrm{d}T_{\mathrm{c}} + \left(\frac{\partial\omega_{\mathrm{SM}}^2}{\partial T}\right)\mathrm{d}V \tag{40}$$

and

$$\mathrm{d}V = -(V/B)\,\mathrm{d}P. \tag{41}$$

Substituting B=53.6 GPa (Zubov and Firsova 1962), $\partial T_{\mathrm{c}}/\partial P$=263.5 K GPa^{-1} (Kravchuk and Tödheide 1996) and $\partial\omega_{\mathrm{SM}}^2/\partial T = 2.122\times10^{-3}(\mathrm{THz})^2\mathrm{K}^{-1}$ (Tezuka et al. 1991) gives an experimental estimate for $\gamma_{\mathrm{V}}^{\mathrm{red}}$(SM)= −15.7 (THz)^2, which agrees poorly with the value from the atomistic lattice dynamics computation of −130.0 (THz)^2 (cf. Table 1). Hence for the soft mode at **k**=0, we find

$$\gamma_{\mathrm{V}}^{\mathrm{red}}(\mathrm{SM, expt.}) = 0.12\,\gamma_{\mathrm{V}}^{\mathrm{red}}(\mathrm{SM, comp.}). \tag{42}$$

There are good grounds from previous experience for believing the general correctness of the interatomic potentials used in the simulation, but there is a substantial difference between the idealised β-structure stabilised at negative pressure at 0 K and v=135.65 Å^3 in the calculations, and the real β-structure at zero pressure, 973 K and v=118.12 Å^3 (Carpenter et al. 1998). One manifestation is the difference in bulk moduli, B^{expt}=56.3 GPa, B^{comp}=133.1 GPa. Also we must remember that the soft mode is 100% anharmonic in the following sense. From the lattice dynamics computation at the volume, 119.43 Å^3, of α-quartz at 0 K, ω_{SM}^2 constrained to the β-phase symmetry P6$_2$22 is

$$\omega_{\mathrm{SM}}^2(T=0)/4\pi^2 = -30.3(\mathrm{THz})^2, \tag{43}$$

while at T_{c} this has increased by +30.3 (THz)^2 due to anharmonic effects:

$$\omega_{\mathrm{SM}}^2(T)/4\pi^2 = -30.3 + 30.3\,T/T_{\mathrm{c}}(\mathrm{THz})^2 \tag{44}$$

Therefore the volume dependences of these anharmonic contributions are equally important to our calculation of γ^{red}. We can carry the argument qualitatively one step further. The first term in Eq. 44 increases algebraically with volume as we have seen, giving the $\gamma_{\mathrm{V}}^{\mathrm{red}}(\mathrm{SM, comp})$ of Eq. 42. The second (anharmonic) term arises from a term $\beta\,\theta^4$ in the total energy due to oxygen ions from different tetrahedra coming into contact at large rotation angles θ. We therefore expect it to decrease (at given θ) as the volume increases, i.e., to have opposite volume dependence to the first term in Eq. 44. The large reduction factor of 0.12 in Eq. 42 shows that the two volume dependences very nearly cancel. Note that the quartic anharmonicity discussed here is quite separate from the cubic anharmonicity responsible for the B term in Eq. 32. We do not expect other modes except this lowest band to be significantly affected in a similar way (Narayanaswamy 1948; Bates and Quist 1972; Castex and Madon 1995).

The TA$_z$ mode along **a***

The TA$_z$ mode is important because it makes the largest negative contribution to the coefficient of expansion as we will see in the Section discussing this topic. But here we concentrate on the TA$_z$ mode for **k** along a*. It is mode 2 for **k** along most of the a* axis (Fig. 5) with a large negative γ^{red} (Fig. 6). As $\gamma^{\mathrm{red}} \propto k^2$ for acoustic modes, and α involves $\gamma = \gamma^{\mathrm{red}}/\omega^2$ where $\omega \propto k$, it is best to work in terms of γ rather than γ^{red}. From Fig. 6 and analogous results for the a, b directions, we deduce

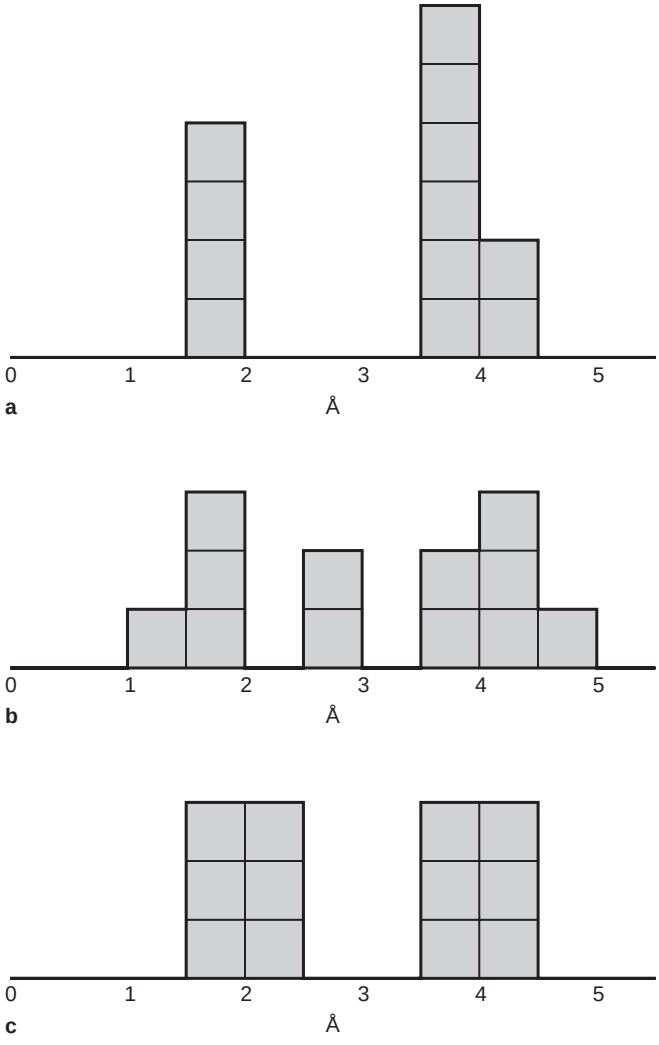

Fig. 7a–c Histogram of oxygen distances from Si atoms in the β-quartz structure, counted in 0.5 Å bins. **a** Undistorted structure with four close oxygen neighbours. **b** and **c** Around two types of Si site after applying an e_5 shear. Note the nearly 6-fold (octahedral) coordination in **c**, with **b** as an intermediate case

$$\tfrac{1}{2}\gamma_{ab} \approx -25 \tag{45a}$$

$$\gamma_c \approx -29. \tag{45b}$$

One interpretation of this large negative γ is in terms of the geometrical constants η. In our rigid unit model, shearing quartz with an e_5=e_4 strain, which corresponds to the TA_z mode, causes a reduction in the a and c lattice parameters as per Eq. 1, with η_a=0.51, η_c=1.74. In Paper I we derive the relationship between η and γ for this acoustic mode,

$$\gamma_a = -\left\{\frac{1}{c_{44}}[(c_{11}+c_{12})\eta_a + c_{13}\eta_c] - \frac{1}{2}\right\} \tag{46a}$$

$$\gamma_c = -\left\{\frac{1}{c_{44}}[2\,c_{13}\eta_a + c_{33}\eta_c] + \frac{1}{2}\right\} \tag{46b}$$

Table 3 Si–O bondlengths in Å in the undistorted β-quartz structure (e_5=0), and around two types of silicon site Si_1 and Si_2 after applying a shear e_5=0.52

e_5=0	Si_1	Si_2
1.58	1.20	1.52
1.58	1.88	1.52
1.58	1.94	1.80
1.58	1.98	2.02
3.71	2.66	2.12
3.71	2.74	2.46
3.87	3.69	3.67
3.87	3.93	3.71
3.87	4.14	3.85
3.87	4.17	4.01
4.14	4.18	4.32
4.14	4.50	4.39

which is analogous to Eq. 36. Using the atomistic computation's elastic constants given below Eq. 37, we obtain $\gamma_a(2)$=−14 and $\gamma_c(2)$=−19. These 'geometrical' values compare reasonably with the computed values quoted above, sufficiently to interpret why they are so large and negative.

We also have another interpretation. For the TA_z mode, we have

$$\omega^2 \propto c_{44}k^2 \tag{47}$$

where c_{44}(=c_{55}) is a positive elastic constant, and the Grüneisen constant

$$\gamma_V \propto -\frac{\partial\omega^2}{\partial V} \propto -\frac{\mathrm{d}c_{44}}{\mathrm{d}V} \tag{48}$$

depends on the stiffness of c_{44} as a function of strain. It turns out that an e_4 type of shear changes the coordination of the silicon atoms from nearly perfect tetrahedral towards octahedral coordination, as documented in Table 3 and in Fig. 7. Now stishovite, the high pressure phase of SiO_2 has octahedral coordination, and hence increase of pressure, thus decrease of volume, favours octahedral coordination. This in turn makes the e_4 shear easier at high pressure, so that it reduces c_{44} and gives a negative γ_V.

This explanation relates to the work of Chelikowsky et al. (Binggeli and Chelikowsky 1991; Keskar and Chelikowsky 1992; Binggeli et al. 1994a, b), who found that the α-quartz structure shows an elastic instability where $(c_{11}-c_{12})\,c_{44}-2\,c_{14}^2$ goes negative when subjected to a pressure of ca. 30 GPa, c_{44} vanishing at ca. 50 GPa. They trace this effect to a TA mode related to a shear which together displace the oxygen atoms into a dense b.c.c. structure (Sowa 1988) with the silicon atoms occupying octahedral interstices. As a result, the Si atoms exhibit an instability between tetrahedral and octahedral coordination. It is the strain coupling which causes the change in the coordination, which is thus largely a geometrical η effect.

The Vallade mode

So far, we have said that low frequency modes make large contributions because of the ω^{-2} factor in γ, we have studied the soft mode (**k**=0) as being easy to picture geomet-

rically, and we have seen in Table 2 that band 1 has a contractive effect. In Fig. 5, with **k** along a^*, the soft mode, SM, mixes with the TA_y mode to form a hybrid mode which we term the Vallade mode, VM, as it was elucidated by Vallade et al. (1992) with respect to the incommensurate phase. Indeed it is in the study of this phase that the detailed study of RUMs started.

If we simply modulate the SM with exp(ikx), we no longer have a RUM. The xy shear (e_6) is also not a rigid unit motion: pure TA_y modes are not RUMs. However an appropriate mixture of the two is a RUM (cf. Fig. 8). The VM is basically a modulated SM (Fig. 2), alternating the angle of rotation $+\theta$, $-\theta$. It is convenient for illustration (Fig. 8) to consider a squared-up wave, with an abrupt change from a constant positive rotation angle θ to $-\theta$ every half-wavelength. The problem occurs at the join, where half a tetrahedron is rotated through $+\theta$ and the other half through $-\theta$. For it to retain its integrity, the $+\theta$ and $-\theta$ regions must be displaced positively and negatively along **b** in Fig. 8, and the tetrahedra on the boundary are rotated about **c**.

To discuss its $\gamma^{\mathrm{red}}_{VM}$, we must first consider ω^2_{VM}, in the same way as in Sect. 3 of Paper I, writing

$$\omega^2 = \frac{\text{coefficient of } \theta^2 \text{ in PE}}{\text{coefficient of } \dot{\theta}^2 \text{ in KE}} \tag{49}$$

as a basic relation of simple harmonic motion. The potential energy, PE, of the $+\theta$ and $-\theta$ regions is exactly equal to that for the. This is true in our squared-up picture, but can easily be extended to sinusoidal modulation. There appears to be zero PE at the boundaries because $\omega^2(\mathrm{VM}\Rightarrow\mathbf{k}\|\mathbf{a}^*)$ is independent of **k** (Fig. 5) and ω^2(VM) and ω^2(SM) both tend to zero at the same volume. Therefore for a given θ, the potential energies per tetrahedron for the VM and SM are equal,

$$\mathrm{PE(VM)=PE(SM)}, \tag{50}$$

if we assume zero contribution from only repositioning of the joining tetrahedra.

The rotational kinetic energy, $\mathrm{KE}^{\mathrm{rot}}_{\mathrm{VM}}$, is equal to that of the SM. Even at the boundary, rotation about the c-axis is of order $\pm\theta$. However, the repositioning of the $+\theta$ and $-\theta$ regions brings in an extra translational kinetic energy

$$\mathrm{KE}^{\mathrm{trans}}_{\mathrm{VM}} = \tfrac{1}{2}(m_{\mathrm{Si}} + 2m_{\mathrm{O}})\dot{y}^2 \tag{51}$$

per tetrahedron, where $y \approx \theta d$ and d is half the length of the side of a tetrahedron in Fig. 8. So we have

$$\mathrm{KE}^{\mathrm{trans}}_{\mathrm{VM}} = \tfrac{1}{2}\left[(m_{\mathrm{Si}} + 2m_{\mathrm{O}})\, d^2\right]\dot{\theta}^2 \tag{52}$$

$$\mathrm{KE}^{\mathrm{rot}}_{\mathrm{VM}} = \tfrac{1}{2}\underbrace{\left[2m_{\mathrm{O}}d^2\right]}_{I}\dot{\theta}^2 \tag{53}$$

and, with Eq. 50,

$$\frac{\omega^2(\mathrm{VM})}{\omega^2(\mathrm{SM})} \approx \frac{2m_{\mathrm{O}}}{2m_{\mathrm{O}} + m_{\mathrm{Si}} + 2m_{\mathrm{O}}} = 0.35 \tag{54}$$

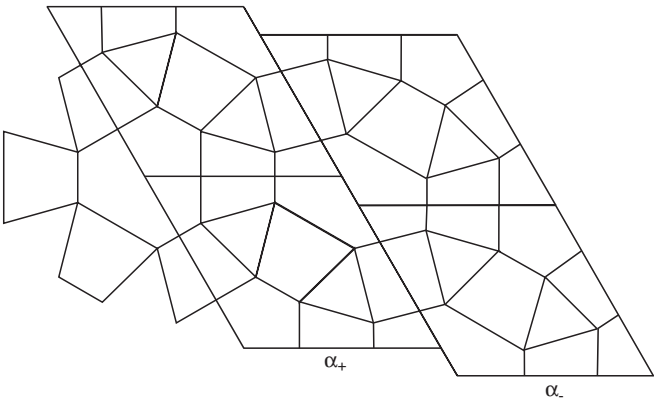

Fig. 8 Squared-up Vallade mode depicted as the soft mode modulated by a square wave TA_y. In the α_+ domain, the soft mode is a rotation through $+\theta$ which is modulated to $-\theta$ in the α_- domain. The tetrahedra on the domain boundary are rotated through arctan sin θ about the c-axis. Note the large relative displacements of the two domains in order for the tetrahedra to join up between them

with m_{O}=16 amu, m_{Si}=28 amu. In fact, from Fig 5, computed values are

$$\frac{\omega^2(\mathrm{VM})}{\omega^2(\mathrm{SM})} \approx \left(\frac{0.422}{0.726}\right)^2 = 0.34, \tag{55}$$

and since ω(SM) and ω(VM) both tend to zero at the same volume, we have

$$\gamma^{\mathrm{red}}(\mathrm{VM}) \approx 0.34\ \gamma^{\mathrm{red}}(\mathrm{SM}). \tag{56}$$

This is in sufficient agreement, considering the semi-quantitative nature of our analysis, with the ratio in Fig. 6

$$\gamma^{\mathrm{red}}(\mathrm{VM})/\gamma^{\mathrm{red}}(\mathrm{SM}) = 40/140 = 0.29. \tag{57}$$

In conclusion, we have interpreted the substantial difference in ωs and γs of the Vallade and soft modes in spite of their rather similar nature. It is due to the displacive inertia effect noted in connection with Eq. 36.

Calculation of thermal expansion

So far we have considered only the Grüneisen parameters. We turn now to the calculation of the thermal expansion coefficients α from the temperature dependent strains (Eq. 17) and stresses (Eq. 18).

In a simple picture with $\omega_{\mathbf{k}j}$ independent of T, and using the high temperature approximation $E_{\mathbf{k}j}=k_{\mathrm{B}}T$, the only term in Eq. 18 which depends on T is $k_{\mathrm{B}}T$. Therefore we can trivially differentiate strain analytically with respect to T to obtain α. The contribution of each band to α is proportional to $\gamma(j)$ (cf. Table 2).

In reality $E_{\mathbf{k}j}(T)$ is more complicated Eq. 14, quantum effects reducing $E_{\mathbf{k}j}(T) - E_{\mathbf{k}j}(T{=}0)$ to less than $k_{\mathrm{B}}T$ and the high temperature approximation not being valid for a few of the highest modes. At T_{c}, $\hbar\omega = k_{\mathrm{B}}T$ for $\omega/2\pi$=17.6 THz, and 22.6 THz for T_{c}+250 K. The highest bands have frequencies around 33 THz. Another compli-

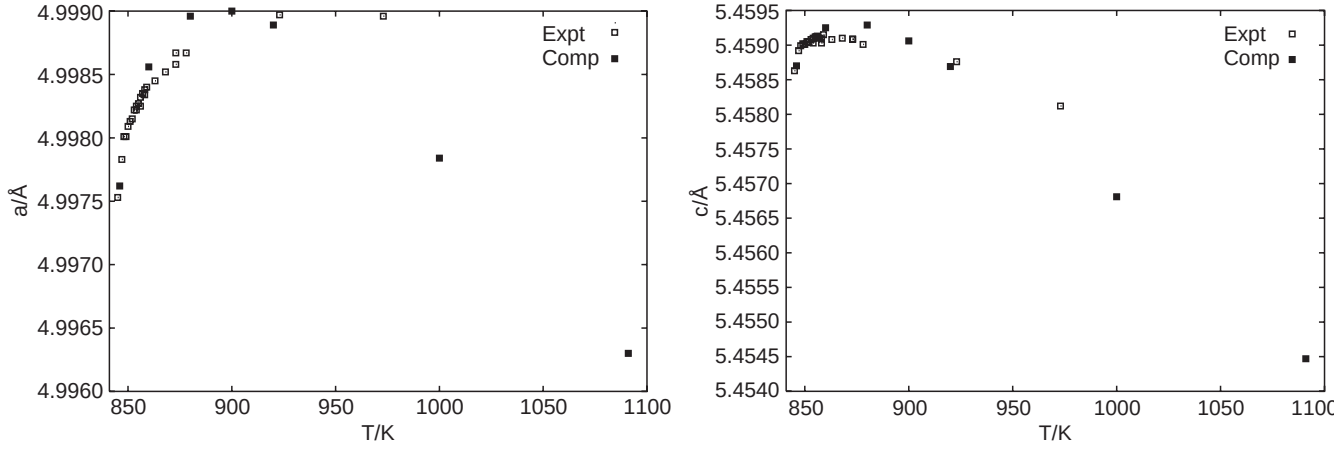

Fig. 9 Comparison of the experimental data (Carpenter et al. 1998) with fitted computed data according to Eq. 58

cation is that ω_{SM}^2 is very temperature dependent. The VM mixes with the acoustic modes, leading to a tangle of crossing and anticrossing in the low frequency phonon spectrum, which from the ω^{-2} weighting factor is the most important region for negative contribution to α. However the temperature dependence of the other mode frequencies gives too small an effect to be significant. For these two reasons it is simplest to calculate $e_a(T)$, $e_c(T)$, thus $a(T)$, $c(T)$ for direct comparison with experiment in Fig. 3. The thermal expansion coefficients can then be found by differencing.

Let us in the present section consider only the region $T \geq 860$ K where $a(T)$ and $c(T)$ vary roughly linearly with temperature. We will return in the next Section to the rapid rise in $a(T)$, $c(T)$ above T_c to $\approx T_c+20$ K which is due to the temperature dependence of ω_{SM}^2 as mentioned qualitatively in the Introduction. For T near to T_c we also had some numerical problems due to ω_{SM}^2 being rather small and partly due to having to marry two quite separate codes for structure relaxation (Busing 1981) and for phonon computation (Pavlides and Catlow 1993), the numerical approximations in the two codes not being consistent.

We recap briefly the computational method from the third section of this paper to obtain strains to compare with the experimental values for the lattice parameters. For a given T, we take ω_{SM} from Eq. 8. The volume, and therefore a and c, are adjusted such that the phonon computation yields the same value $\omega_{SM}(T)$. We then calculate $\omega_{\mathbf{k}j}$ at (a, c), $(a+\delta a, c)$, $(a, c+\delta c)$ and difference to obtain $\gamma_a^{red}(\mathbf{k}j)$, $\gamma_c^{red}(\mathbf{k}j)$. These are weighted by the mode's $E(T)$ and summed over k-space according to Eq. 18 to give thermal stresses using the k-space sampling Eq. 30 with $N_s=70$. The stresses combined with the elastic constants yield thermal strains and thus the temperature dependence of the lattice parameters.

The computations for the modes $j=2$ to 27 are straightforward, and give thermal stresses which very nearly vary linearly with temperature. For the sum of the acoustic modes $j=2$ to 4, this variation $d\xi/dT=(-1.4, -1.5) \times 10^6$ Jm^{-3} K^{-1} is hugely negative, and as we shall see later is mainly from the TA_z mode. The other modes together make a net positive contribution increasingly linearly with temperature of gradient $(7.9, 7.5)\times 10^5$ Jm^{-3} K^{-1}. As we will see in the following section, $\xi(j=1)$, which is mainly due to the soft mode, is the band which gives the lattice parameters' variation with temperature its characteristic shape.

From Eq. 42 we saw that the contribution from the soft mode is grossly overestimated in our computer model using an expanded β-quartz structure. The computed γ_{SM}^{red} has to be reduced by a factor 0.12 which will feed through to the contribution to the thermal stress. Clearly not all of band 1 needs to be reduced by as much as that, but most of it is like the soft mode or the Vallade mode, so that the reduction factor will still be of that order of magnitude. We can refine it by fitting computed lattice parameters

$$a_t = a_t^0(1+e_t), \tag{58}$$

where e_t is found from Eq. 17 and

$$\xi_{ab}=A_{ab}\xi_{ab}(j=1)+\xi_{ab}(j=2 \text{ to } 27), \tag{59a}$$

$$\xi_c=A_c\xi_c(j=1)+\xi_c(j=2 \text{ to } 27) \tag{59b}$$

to the experimental lattice parameters of Fig. 3, with A_s and a_t^0 as fit parameters. This fit is shown in Fig. 9 with $A_{ab}=0.24$ and $A_c=0.15$. We see from Fig. 9 that this gives a good account of the overall shape and variation of $a(T)$, $c(T)$ except that the negative coefficient of expansion of $a(T)$ at high T is overestimated.

Contribution of soft mode band near T_c

We now bring together several points already mentioned previously connected with the soft mode and the lowest phonon band $j=1$ connected with it. The strong temperature dependence of ω^2 in Eq. 18 for the SM/VM reverses the sign of its contribution to α. It is also the cause of the big rise in a, c above T_c. We shall explain this big rise in terms of our quasi-harmonic theory. It is not due to some extra critical fluctuations and not evidence of some abnormal structure such as one made up of domains of α_+, α_--quartz. We will by-pass the numerical problems with the

computation near T_c with an analytic model. At the end we consider whether the temperature dependence of the frequencies of the other modes makes a significant contribution.

Let us first very simply consider the contribution to the strain from the SM itself,

$$e_{SM} \propto -\frac{T}{T-T_c}\left|\gamma_{SM}^{red}\right| \tag{60}$$

where the numerator comes from $E_{\mathbf{k}j}=k_B T$ and the denominator is $\omega_{SM}^2(T)$ from Eq. 8. The soft mode's γ^{red} is negative, so we have taken its sign out explicitly in front. We conclude that the contribution to δa, δc is negative, but decreasing rapidly in magnitude as temperature increases, yielding a large positive contribution to α:

$$\frac{de}{dT} \propto +\frac{T_c}{(T-T_c)^2}\left|\gamma_{SM}^{red}\right|. \tag{61}$$

This provides a qualitative explanation for the experimental data at $T \geq T_c$ in Fig. 3.

To estimate the total effect, as Eq. 18 involves a summation over the Brillouin zone, we need to construct a model of $\omega_{\mathbf{k}}^2$ for the band which has the nature of the SM distortion. As mentioned in the Section on the Vallade mode, the SM exists strictly speaking at $\mathbf{k}$=0 only, but a mixture of it with TA_y known as the VM goes soft as well and exists along $\langle 100\rangle$. Similarly, the lowest mode along $\langle 001\rangle$ has SM nature. Along these directions ω is roughly constant, much as a valley floor, as for the VM, the lowest band in Fig. 5. Away from these directions, ω rises steeply and quadratically (at least initially), and we write

$$\omega^2(\mathbf{k}) \approx m k_\perp^2 + B(T-T_c) \tag{62}$$

where $k_\perp$ is the component of $\mathbf{k}$ perpendicular to the $\mathbf{a}^*(\Sigma)$ or $\mathbf{c}^*(\Delta)$ axis and B defines the "height" of the "valley floor". The values of m were taken as the average of two perpendicular directions at $\frac{1}{2}a^*$ and $\frac{1}{2}c^*$ respectively. The integration over the Brillouin zone is in turn approximated by an integration over three cylinders along $\langle 100\rangle$ (Σ) and one along $\langle 001\rangle$ (Δ) whose total volume is made equal to $(2\pi)^3/v$ by adjusting their radius ρ. After applying these approximations, Eq. 18 becomes for i=ab, c

$$\begin{aligned}\xi_i(j=1) &= \frac{3a^* k_B T}{(2\pi)^3}\gamma_{i,\Sigma}^{red}\int_0^\rho \frac{2\pi k\,dk}{m_\Sigma k^2 + B_\Sigma(T-T_c)} \\ &\quad + \frac{c^* k_B T}{(2\pi)^3}\gamma_{i,\Delta}^{red}\int_0^\rho \frac{2\pi k\,dk}{m_\Delta k^2 + B_\Delta(T-T_c)} \\ &= \frac{3a^* k_B T}{8\pi^2}\frac{\gamma_{i,\Sigma}^{red}}{m_\Sigma}\ln\left(1+\frac{m_\Sigma\rho^2}{B_\Sigma(T-T_c)}\right) \\ &\quad + \frac{c^* k_B T}{8\pi^2}\frac{\gamma_{i,\Delta}^{red}}{m_\Delta}\ln\left(1+\frac{m_\Delta\rho^2}{B_\Delta(T-T_c)}\right).\end{aligned} \tag{63}$$

Substituting values we have

Table 4 Experimental values of $\omega(T)/2\pi$ in THz for Raman active modes in β-quartz

853 K[a]	873 K[a]	923 K[a]	933 K[b]	973 K[c]
0.16[SM d]	0.26[SM d]	0.42[SM d]	0.44[SM d]	0.53[SM d]
2.94	2.94	2.94	2.91	2.94
~4.95	~4.95	~4.95		
~7.40	~7.31	~7.28	7.49	7.28
12.16	12.21	12.22	11.84	12.20
				12.80
13.73	13.75	13.79	13.57	13.91
?	~20.42	~20.54	~20.57	20.57
23.92	23.91	23.91	23.74	23.56
?	?	?	~31.78	31.93
34.96	35.06	34.98	34.60	35.17
?	~36.75	~36.69		36.87

[a] Castex and Madon (1995).
[b] Narayanaswany (1948).
[c] Bates and Quist (1972).
[d] Soft mode frequencies calculated from Tezuka et al. (1991) for comparison.

$$\begin{aligned}\xi_c(j=1) = &-2.57\times10^5 T\ln\left(1+\frac{1.95\times10^4}{(T-T_c)}\right) \\ &-1.09\times10^5 T\ln\left(1+\frac{1.51\times10^4}{(T-T_c)}\right)\end{aligned} \tag{64a}$$

and

$$\begin{aligned}\xi_{ab}(j=1) = &-4.77\times10^5 T\ln\left(1+\frac{1.95\times10^4}{(T-T_c)}\right) \\ &-1.76\times10^5 T\ln\left(1+\frac{1.51\times10^4}{(T-T_c)}\right).\end{aligned} \tag{64b}$$

Computed values from Eq. 64 fit the form of a single term

$$\xi = -\kappa T\ln\left(1+\frac{\varepsilon}{T-T_c}\right) \tag{65}$$

well, where κ and ε are positive constants, which exhibits the overall form of Eq. 64. It has the limiting behaviour $\lim_{T\to T_c^+}\xi\to-\infty$, $\lim_{T\to\infty}\xi\to-\kappa\varepsilon$ with a maximum at about T_c+250 K. So it is this lowest band which gives the overall shape of the lattice parameters' variation in temperature, notably the rise above T_c, with a peak, and makes a negative contribution to α at high temperature.

The analytic $\xi(j$=1) of Eq. 64 was added to the linear contributions from the other modes in Eq. 59 and again fitted to experimental data, again with correction factors A_{ab}, A_c applied to Eq. 63 for the j=1 band. These factors include the 0.12 of Eq. 42, the 0.29 of Eq. 57, and all other variation of $\gamma_{ab,c}^{red}(\mathbf{k}, j=1)$ and $\omega^2(\mathbf{k}, j$=1) through the band. The results with A_{ab}=0.05 and A_c=0.08 are shown in Fig. 10. We see that the rapid rise in $a(T)$, $c(T)$ just above T_c is reproduced very well, from which we conclude that this rise can be accounted for by simple classical quasi-harmonic theory without critical fluctuations or more exotic models.

Let us return to the temperature dependence of the other modes: does this also make a significant contribution to

α? We have ignored it so far and have even put in a spurious $\omega^2(T_{\rm eff})$ by tuning volume to $\omega^2_{\rm SM}(T)$. There are a few experimental data of $\omega(T, \mathbf{k}{=}0)$ for Raman active modes given in Table 4. Let us write

$$\omega^2(T){=}\omega^2(T_{\rm c}){+}B(T{-}T_{\rm c}). \tag{66}$$

For a mode with negative $\gamma^{\rm red}$, the strain and coefficient of thermal expansion are proportional to the following:

$$e \propto -\frac{T}{\omega^2(T_{\rm c})+B(T-T_{\rm c})}\left|\gamma^{\rm red}\right|, \tag{67a}$$

$$\alpha \propto \frac{-\omega^2(T_{\rm c})+BT_{\rm c}}{\left[\omega^2(T_{\rm c})+B(T-T_{\rm c})\right]^2}\left|\gamma^{\rm red}\right|. \tag{67b}$$

The point is that B for the other modes is not very different from that of the SM (Eq. 8) as shown in Table 4. The major difference is that $\omega^2(T_{\rm c}){=}0$ for the SM but is large compared to $BT_{\rm C}$ for all the others. Therefore we are justified in ignoring the temperature dependence of ω^2 except in the case of the soft mode and can safely introduce a small spurious $\omega^2(T_{\rm eff})$ into our computer model.

Discussion of the TA_z contribution

We have already seen in a previous Section that the TA_z mode's γ along a^* is strongly negative, but what about its total contribution to α? The TA_z mode is only a RUM over the a^* b^* plane. It is among the four lowest modes over the whole Brillouin zone which interact strongly with each other away from special symmetry and RUM directions. This makes the individual contribution of each type of mode hard to disentangle, but we can make an estimate based on the γ parameters calculated along the a^* axis where the modes mostly do not mix. As mentioned above, it is best to work in terms of γ rather than $\gamma^{\rm red}$ for acoustic modes. Then the k-space summation in Eq. 18 just gives a factor of N. We have

$$\xi{\approx}k_{\rm B}T\gamma/\upsilon, \tag{68}$$

from which the coefficients of linear expansion $\alpha_{\rm a}$, $\alpha_{\rm c}$ can be derived using Eqs. 17 and 19. Along the a^* axis, the pure TA_z mode can be identified from Fig. 5 and from its eigenvector. The Grüneisen parameters are shown in Table 5, giving $(\alpha_{\rm a}, \alpha_{\rm c})\,(TA_z){=}(-14.8, -17.5){\times}10^{-6}\ {\rm K}^{-1}$ as the total contribution from xz shear type of transverse motion from all modes. This is by far the largest negative contribution to α and more or less cancels all positive contributions. Indeed experimentally from Fig. 3 we have $(\alpha_{\rm a}, \alpha_{\rm c}){\approx}(-2,0){\times}10^{-6}\ {\rm K}^{-1}$ at temperatures well above $T_{\rm c}$ where the anomalous contribution from the soft mode has more or less died out and we can ascribe these negative values as ultimately due to the TA_z component.

The other true acoustic mode is the longitudinal one (LA), and there is the mixed mode $SM/TA_y)_+$ which is orthogonal to the Vallade mode and is acoustic-like everywhere except very close to $\mathbf{k}{=}0$ in Fig. 5 (Tautz et al. 1991; Vallade et al. 1992). These have the Grüneisen parameters shown in Table 5, much smaller than those of the TA_z mode, and give a proportionately smaller contribution to $\alpha_{\rm a}$, $\alpha_{\rm c}$.

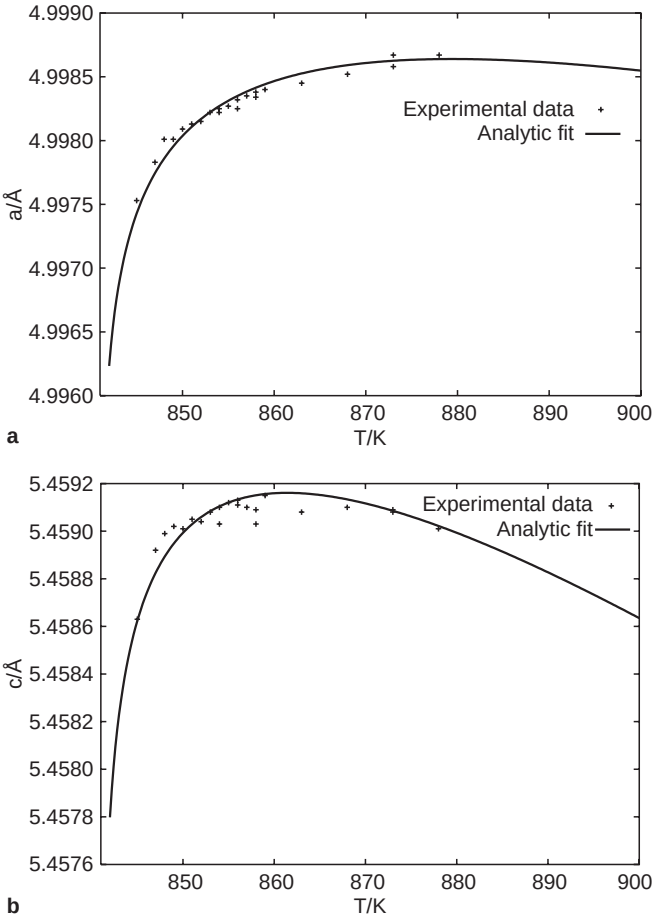

Fig. 10a, b Comparison between experimental data and analytic expression from Eq. 64

Table 5 Grüneisen parameters for the acoustic modes for $\mathbf{k}$ along the a^* axis

Mode	$\frac{1}{2}\gamma_{\rm ab}$	$\gamma_{\rm c}$
TA_z	−24.9	−28.6
LA	−3.0	−3.6
$(SM/TA_y)_+$	−3.5	−3.4

The three acoustic modes get mixed over most of the Brillouin zone, as already remarked, but we can check the consistency of our picture by noting that the sum of the values in Table 2 for bands 2, 3 and 4 is very roughly equal to the sum of the three values in Table 5.

Conclusions and discussion

The theory and experimental data for -quartz are complicated by the soft mode, but in spite of that the geometrical rotational origin of negative thermal expansion has been clearly documented in accordance with the qualitative picture in Fig. 1 and Eqs. 1 and 4. Well above $T_{\rm c}$ it can-

cels the normal positive anharmonic effect to give approximately zero or even slightly negative expansion. The reduced Grüneisen parameters calculated for the soft mode agree satisfactorily with those expected from the geometrical η_{ab}, η_c constants, and the same is true of the TA_z mode.

Three aspects of the results were unanticipated but then satisfactorily explained. As well as adding to our understanding of β-quartz, they may be expected to have analogues in other materials. The first point is that negative Grüneisen constants and hence negative contributions to thermal expansion are not the preserve of a few phonon modes which are RUMs and have very low frequencies. In fact nearly half the bands with **k** along a^* have negative $\gamma^{red}(\mathbf{k}\,j)$, although the lowest ones give the largest contribution to the expansion because of the $\omega_{\mathbf{k}j}^{-2}$ weighting factor. The reason is that most phonons contain a substantial rotational part. If we ignore the internal vibration of the Si atom in a tetrahedron, each tetrahedron has three translational and three rotational degrees of freedom so that we may picture the character of phonons to be about half rotational in general throughout the whole phonon spectrum. This means that the geometrical negative contribution to $\gamma^{red}(\mathbf{k}\,j)$ is broadly of constant magnitude across the whole of the phonon spectrum. More detailed theory (Heine et al. 1998) shows that the anharmonicity of the interatomic potential contributes to $\gamma^{red}(\mathbf{k}\,j)$ an amount proportional to $\omega_{\mathbf{k}j}^2$. Thus the geometrical rotational part dominates at low ω and the anharmonicity dominates for phonons of high frequency, which explains the systematic variation of $\gamma^{red}(\mathbf{k}\,j)$ from negative to positive through the spectrum.

A second unexpected point was the dominant negative contribution of the TA_z modes. These are RUMs and hence have low frequency: the tetrahedra `roll over one another' as one applies an xz or yz shear to the crystal. But another aspect also helps to reduce the elastic constant c_{55} and hence the frequencies of the TA_z modes, which boosts the ω^{-2} weighting factor: an xz shear tends to alter the coordination of oxygen atoms around a Si from tetrahedral towards octahedral, which is known also to be energetically favourable in the high pressure phases. This effect is effectively the same as that found by Chelikowsky in the behaviour of the elastic constants of α-quartz under high pressure.

The most important general lesson concerns the soft mode. It is a RUM and has negative γ_{ab}^{red}, γ_c^{red} in accordance with the geometrical rotational interpretation. But the temperature variation of the soft mode frequency changes the sign of the contribution to the coefficient of expansion. We can see this simply as follows. The contibution to the lattice parameters is negative and proportional to

$$k_B T \gamma^{red} / \omega_{SM}{}^2(T) \tag{69}$$

as usual. But the point is how it varies with temperature. The $\omega^2(T)$ increases with T, so that the whole expression (Eq. 69) becomes less negative with increasing T, i.e., one has a positive coefficient of expansion. Because $\omega_{SM}^2(T)$ starts at zero at $T{=}T_c$, it increases proportionally much more rapidly with T than the numerator of Eq. 69 does and hence it dominates the temperature variation. Eq. 69 is proportional to

$$\frac{T}{T - T_c}\gamma^{red} \tag{70}$$

and differentiating with respect to T demonstrates the change of sign from a negative expansion to a positive coefficient of expansion.

We also saw that the soft mode is troublesome in other ways. The lattice dynamical calculations are effectively done at zero Kelvin, where the β-quartz structure is unstable and the calculated ω_{SM}^2 is negative. The soft mode is therefore exceedingly anharmonic, reaching positive ω_{SM}^2 above T_c. For this reason the computed γ^{red} for the soft mode do not agree well with the experimental values deduced from dT_c/dP, differing by a factor 0.12.

References

Ashcroft NW, Mermin ND (1981) Solid state physics. Holt-Saunders, Tokyo

Bates JB, Quist AS (1972) Polarized Raman spectra of β-quartz. J Chem Phys 56:1528–1533

Binggeli N, Chelikowsky JR (1991) Structural transformation of quartz at high pressures. Nature 353:344–346

Binggeli N, Chelikowsky JR, Wentzcovitch RM (1994a) Simulating the amorphization of α-quartz under pressure. Phys Rev B 49:9336–9340

Binggeli N, Keskar NR, Chelikowsky JR (1994b) Pressure-induced amorphization, elastic instability, and soft modes in α-quartz. Phys Rev B49:3075–3081

Busing WR (1981) Wmin, a computer program to model molecules and crystals in terms of potential energy functions. Technical Report ORNL-5747, Oak Ridge National Laboratory

Carpenter MA, Salje EKH, Graeme-Barber A, Wruck B, Dove MT, Knight KS (1998) Calibration of excess thermodynamic properties and elastic constant variations due to the $\alpha \leftrightarrow \beta$ phase transition in quartz. Am Mineral 83:2–22

Castex J, Madon M (1995) Test of the vibrational modeling for the lambda-type transitions – application to the alpha-beta quartz transition. Phys Chem Minerals 22:1–10

Dolino G, Berge B, Vallade M, Moussa F (1992) Origin of the incommensurate phase of quartz: I. Inelastic neutron scattering study of the high temperature β phase of quartz. J Physique I 2:1461–1480

Dove MT (1993) Introduction to lattice dynamics. (Cambridge topics in mineral physics and chemistry, vol 4). Cambridge University Press, Cambridge, UK

Dove MT, Giddy AP, Heine V (1991) Rigid unit mode model of displacive phase transitions in framework silicates. Trans Am Crystallogr Assoc 27:65–74

Dove MT, Giddy AP, Heine V (1992) On the application of mean-field and Landau theory to displacive phase transitions. Ferroelectrics 136:33–49

Dove MT, Heine V, Hammonds KD (1995) Rigid unit modes in framework silicates. Mineral Mag 59:629–639

Dove MT, Hammonds KD, Heine V, Withers RL, Xiao Y, Kirkpatrick RJ (1996) Rigid unit modes in the high-temperature phase of SiO_2 tridymite – calculations and electron-diffraction. Phys Chem Minerals 23:56–62

Dove MT, Harris MJ, Hannon AC, Parker JM, Swainson IP, Ghambir M (1997) Floppy modes in crystalline and amorphous silicates. Phys Rev Lett 78:1070–1073

Downs RT, Gibbs GV, Bartelmehs KL, Boisen Jr MB (1992) Variations of bond lengths and volumes of silicate tetrahedra with temperature. Am Mineral 77:751–757

Evans JSO, Hu Z, Jorgensen JD, Argyriou DN, Short S, Sleight AW (1997) Compressibility, phase transitions and oxygen migration in zirconium tungstate, ZrW_2O_8. Science 275:61–65

Grimm H, Dorner B (1975) On the mechanism of the α-β phase transformation of quartz. J Phys Chem Solids 36:407–413

Hammonds KD, Dove MT, Giddy AP, Heine V, Winkler B (1996) Rigid unit phonon modes and structural phase transitions in framework silicates. Am Mineral 81:1057–1079

Hammonds KD, Deng H, Heine V, Dove MT (1997a) How floppy modes give rise to adsorption sites in zeolites. Phys Rev Lett 78:3701–3704

Hammonds KD, Heine V, Dove MT (1997b) Insights into zeolite behaviour from the rigid unit mode model. Phase Transitions 61:155–172

Hammonds KD, Heine V, Dove MT (1998c) Rigid unit modes and the quantitative determination of the flexibility possessed by zeolite frameworks. J Phys Chem B102:1759–1767

Heine V, Welche PRL, Dove MT (1998) Geometrical origin and theory of negative thermal expansion in framework structures. Am Ceram Soc (in press)

Hochella MF Jr, Brown GE Jr (1986) Structural mechanisms of anomalous thermal expansion of cordierite-beryl and other framework silicates. J Am Ceram Soc 69:13–18

Hummel FA (1984) A review of thermal expansion data of ceramic materials, especially ultra-low expansion compositions. Interceram, 33:27–30

Keskar NR, Chelikowsky JR (1992) Negative poisson ratios in crystalline SiO_2 from first principles calculations. Nature 358:222–224

Korthuis V, Khosrovani N, Sleight AW, Roberts N, Dupree R, Warren Jr WW (1995) Negative thermal expansion and phase transitions in the $ZrV_{2-x}P_xO_7$ series. Chem Mater 7:412–417

Kravchuk KG, Tödheide K (1996) Solid-liquid-vapor equilibria in water-salt systems – a DTA study at elevated temperatures and pressures. Z Phys Chem 193:139–150

Leibfried G, Ludwig W (1961) Theory of anharmonic effects in crystals. In: Seitz F, Turnbull D (eds) Solid state physics, vol 12. Academic Press, New York, p 335

Megaw HD (1973) Crystal structures: a working approach (Studies in physics and chemistry, no 10). W B Saunders Company, Philadelphia

Narayanaswamy PK (1948) The α-β transformation in quartz. Proc Indian Acad Sci A28:417–422.

Pavlides P, Catlow CRA (1993) Elastic-constants and lattice-vibrations of CO_2 and C_6H_6. Mol Phys 79:1025–1036

Pryde AKA, Hammonds KD, Dove MT, Heine V, Gale JD, Warren MC (1996) Origin of the negative thermal expansion in ZrW_2O_8 and ZrV_2O_7. J Phys Condens Matter 8:10973–10982

Schulz H (1974) Thermal expansion of beta eucryptite. J Am Ceram Soc 57:313–318

Sowa H (1988) The oxygen packings of low-quartz and ReO_3 under high-pressure. Z Krist 184:257–268

Tautz FS, Heine V, Dove MT, Chen X (1991) Rigid unit modes in the molecular dynamics simulation of quartz and the incommensurate phase transition. Phys Chem Minerals 18:326–336

Tezuka Y, Shin S, Ishigame M (1991) Observation of the silent phonon in beta-quartz by means of hyper-raman scattering. Phys Rev Lett 66:2356–2359

Tscherry V, Schulz H, Czank M (1972) Thermal expansion of lattice constants of β-eucryptite single crystals. Ber Deut Keram Ges 49:153–154

Tsuneyuki S, Tsukada M, Aoki H, Matsui Y (1988) First-principles interatomic potential of silica applied to molecular dynamics. Phys Rev Lett 61:869–872

Vallade M, Berge B, Dollino G (1992) Origin of the incommensurate phase of quartz: II. Interpretation of inelastic neutron scattering data. J Physique I 2:1481–1495

Zubov VG, Firsova MM (1962) Elastic properties of quartz near the α-β transition. Sov Phys Cristallogr 7:374–376